PLANT SCIENCES

Non-adapted bacterial infection suppresses plant reproduction

Jing-Ting Yang[1]†, Zhi-Min Tan[1,2]†, Yu-Tong Jiang[1,3]†, Yu-Xuan Bai[4], Yan-Jie Zhang[1], Hong-Wei Xue[3,5], Tong-Da Xu[6], Tao Dong[1,2]*, Wen-Hui Lin[1]*

Environmental stressors, including pathogens, substantially affect the growth of host plants. However, how non-adapted bacteria influence nonhost plants has not been reported. Here, we reveal that infection of *Arabidopsis* flowers by *Xanthomonas oryzae* pv. *oryzae* PXO99A, a bacterial pathogen causing rice blight disease, suppresses ovule initiation and reduces seed number without causing visible disease symptoms. TleB, secreted by the type VI secretion system (T6SS), interacts with plant E3 ligase PUB14 and disrupts the function of the PUB14-BZR1 module, leading to decreased ovule initiation and seed yield. On the other site, PUB14 concurrently promotes TleB's degradation. Our findings indicate that bacterial infections in nonhost plants directly repress offspring production. The regulatory mechanism by effectors PUB14-BZR1 is widely present, suggesting that plants may balance reproduction and defense and produce fewer offspring to conserve resources, thus enabling them to remain in a standby mode prepared for enhanced resistance.

INTRODUCTION

A close connection exists between bacteria and host plants, and bacteria can evolve a variety of mechanisms to enhance their ability to infect, colonize, and interact with host plants. For nonhost plants, plants resist bacterial infection through pattern-triggered immunity (PTI), effector-triggered immunity, and hypersensitive response (*1*, *2*). However, the specific effects of non-adapted pathogen infection on nonhost plants and the response of nonhost plants remain unclear. Previous studies revealed that arbuscular mycorrhizal fungi (AMF) can infect nonhost plants, then rob nutrients, and inhibit the growth and development of nonhost plants, while AMF can successfully establish symbiosis with host plants (*3*). However, the interaction between bacteria and nonhost plants remains to be explored.

Plants maintain a delicate balance between growth and immunity to navigate adverse environmental challenges, such as pathogen attacks or insect herbivory. This balance is crucial for maximizing survival (*4*–*7*). During growth and development, plants activate their defense systems in response to diseases and pests, which, while necessary, suppresses both vegetative and reproductive growth, ultimately affecting crop yield in terms of both quality and quantity of seeds. Traditionally, research on plant responses to environmental stressors has predominantly used leaves, with limited focus on the biological stress impacts directly affecting reproductive organs (*8*).

Ovules are precursors of seeds. Ovule initiation has great impact on seed number and yield. Our previous studies have revealed that ovules initiate in multiple rounds, providing an opportunity to adjust offspring number based on environmental conditions (*9*, *10*). It is well established that plant hormones, especially auxin, cytokinin (CK), brassinosteroid (BR), and gibberellin (GA), are integral to regulating ovule and seed numbers (*9*–*15*). Our previous publications demonstrated that BRASSINAZOLE RESISTANT 1 (BZR1) directly regulates ovule initiation and ovule number through multiple mechanisms including promoting placenta elongation, transcriptional regulating ovule-related genes, and enhancing auxin and CK signaling (*9*–*11*, *14*). However, the environmental regulation of ovule initiation remains largely unexplored and presents a substantial gap in our understanding of plant reproductive biology.

Here, we uncover a phenomenon that non-adapted pathogen, *Xanthomonas oryzae* pv. *oryzae* PXO99A (PXO99A), infects nonhost plant *Arabidopsis* and results in repressed ovule initiation and reduced seed number. The E3 ubiquitin ligase PLANT U-BOX 14 (PUB14) in *Arabidopsis*, a U-box family protein, is a crucial mediator for the repressed reproduction during bacterial infection. Under normal conditions, PUB14 interacts with and stabilizes BZR1, enhancing ovule initiation and positively influencing seed numbers. Upon infection with PXO99A, PUB14 rapidly binds to and ubiquitinates the bacterial effector type VI lipase effector (TleB), facilitating its degradation via the 26*S* proteasome. This interaction disrupts the association between PUB14 and BZR1, leading to reduced BZR1 abundance and impaired ovule initiation, thereby changing the plant status from normal to standby for defense. *Arabidopsis* prepares its defense by increasing transcription of PTI genes although *Arabidopsis* does not illustrate obvious response for disease resistance. Because the seed is the sink, the reduced seed number leaves more carbohydrates in other plant tissues and organs, which is beneficial for bacteria, and guarantees the survival of the plant itself and the existing seeds. It may be a compromise strategy of nonhost plants to the unfriendly environment with bacteria, which means that plants repress their reproductive fitness to standby to defend against bacterial infection.

RESULTS

Bacteria inhibit ovule initiation and lead to decreased ovule number

To investigate the direct impact of biotic stress on plant reproductive development and seed formation, we infected the inflorescence

[1]School of Life Sciences and Biotechnology, Joint International Research Laboratory of Metabolic and Developmental Sciences, Shanghai Jiao Tong University, Shanghai 200240, China. [2]Department of Immunology and Microbiology, School of Life Sciences, Southern University of Science and Technology, Shenzhen 518055, Guangdong, China. [3]Shanghai Collaborative Innovation Center of Agri-Seeds/Joint Center for Single Cell Biology, School of Agriculture and Biology, Shanghai Jiao Tong University, Shanghai 200240, China. [4]Zhiyuan College, Shanghai Jiao Tong University, Shanghai 200240, China. [5]Guangdong Laboratory for Lingnan Modern Agriculture, College of Agriculture, South China Agricultural University, Guangzhou 510642, China. [6]Haixia Institute of Science and Technology, Fujian Agriculture and Forestry University, Fuzhou 350007, China.
*Corresponding author. Email: whlin@sjtu.edu.cn (W.-H.L.); dongt@sustech.edu.cn (T.D.)
†These authors contributed equally to this work.

apices of wild-type *Arabidopsis* (Col-0) with three common bacterial strains for 3 hours: *Pseudomonas syringae* pv. *tomato* DC3000 (DC3000), *Acidovorax citrulli* (AC), and *Xanthomonas oryzae* pv. *oryzae* PXO99A (PXO99A) (fig. S1A) (*16*). After infection, we allowed the flowers to grow for 14 days before harvesting siliques to measure the length of mature silique and total seed count. Our phenotypic analysis revealed that DC3000 notably inhibited flower development and eventually caused wilting, resulting in no seed production. Flowers infected with PXO99A did not wilt but exhibited a significant reduction in silique length (Fig. 1E). In addition, the infection with AC caused a small number of wilt flowers as well as some shorter siliques (fig. S1B). Thus, we observed these cleared pistils by differential interference contrast (DIC) microscope and dissected these siliques infected with PXO99A and found a marked reduction in total seed count, including both healthy and aborted seeds (Fig. 1, A to E). Then, we did the dose inoculation experiments for PXO99A to determine the infection threshold to cause the reduction in total seed count. We counted the number of ovules (seed precursors) after the infection with different concentrations of PXO99A. The results revealed that the repression of ovule initiation and reduced

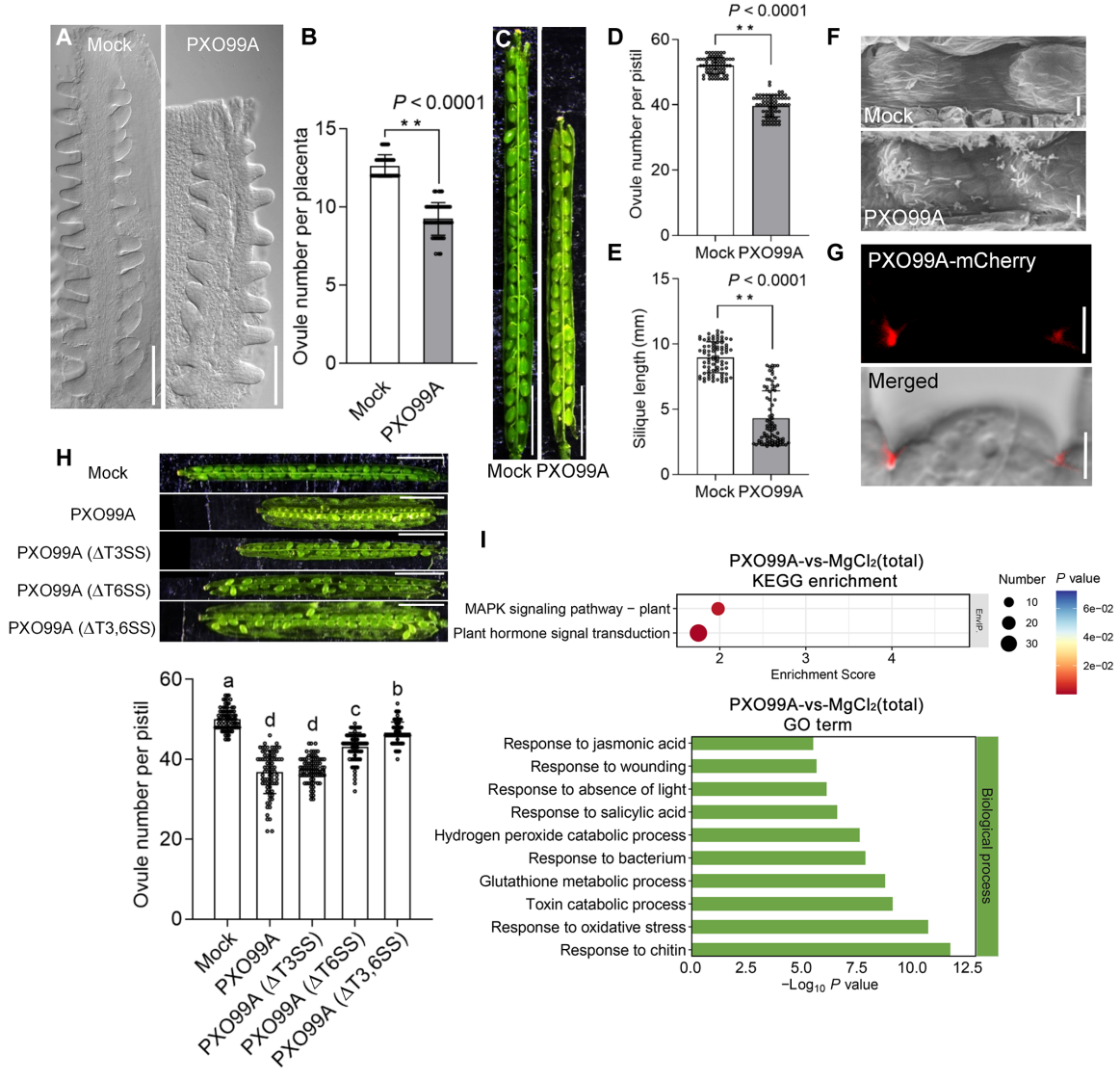

Fig. 1. Non-adapted bacterial infection inhibits ovule initiation through T6SS. (**A** and **B**) Phenotypic analysis of placenta length and statistical analysis of ovule number per placenta after PXO99A infection. Scale bars, 100 μm. Bars represent means ± SD of three biological replicates ($n = 50$). (**C** to **E**) Phenotypic and statistical analysis of ovule number per pistil and silique length after PXO99A infection. Scale bars, 2 mm. Bars represent means ± SD of three biological replicates. Ovule number per pistil ($n = 70$) and silique length ($n = 80$). (**F**) Scanning electron microscopy (SEM) observation of bacteria on the placenta and ovule primordia. Scale bars, 5 μm. (**G**) Bacteria with fluorescent marker localize on ovule boundaries. Scale bars, 5 μm. (**H**) Phenotypic and statistical analysis of ovule number per pistil after infection of PXO99A, PXO99A (ΔT3SS), PXO99A (ΔT6SS), and PXO99A (ΔT3,6SS). Scale bars, 2 mm. Bars represent means ± SD of three biological replicates ($n = 80$). (**I**) Kyoto Encyclopedia of Genes and Genomes (KEGG) enrichment and Gene Ontology (GO) term analysis of differentially expressed genes (DEGs) (PXO99A versus $MgCl_2$) in transcriptome analysis. Asterisks indicate significant difference (Student's two-tailed *t* test, $^{**}P < 0.01$). Lowercase letters indicate significant differences among different stages [one-way analysis of variance (ANOVA), $P < 0.05$].

seed quantity are related to bacterial concentration. Bacterial infection in very low concentration [optical density (OD) of 10^{-3}] could lead to reduced ovule number (the most significant decrease was observed at OD of 1.0), indicating the possible natural infection threshold of bacteria to cause the flower phenotype in *Arabidopsis* (fig. S1C). These results suggest that different bacterial infections lead to distinct phenotypes, with PXO99A treatment resulting in non-pathogenic phenotypes characterized by reduced ovule initiation and decreased seed set.

Previous studies have indicated that PXO99A is a non-adapted pathogen for *Arabidopsis*, and plants infected with PXO99A show normal vegetative growth without overall defects (*17*). Therefore, PXO99A is suitable for studying the impact of bacteria on nonhost plant reproductive development. We used scanning electron microscopy (SEM) and confocal microscopy to examine pistils treated with PXO99A and mCherry-labeled PXO99A (Fig. 1, F and G). The results demonstrated that PXO99A bacteria targeted the placentae and ovule primordia. Fluorescence signals in these tissues indicated that PXO99A might directly influence ovule initiation rather than indirectly affecting overall plant growth and development (Fig. 1, G and H). In addition, to investigate the possible sources of microorganisms in *Arabidopsis*, we collected various insects in our greenhouse and conducted metagenomic sequencing to explore the microbial population in insects. The results of microbial community annotation were visualized using Krona analysis, and results showed that the insects contained various bacteria (*18*), including *Xanthomonas oryzae* (to which PXO99A belongs), suggesting that insects might facilitate the transfer of bacteria among different plant species (both host and nonhost) and PXO99A might reach the pistil and affect ovule initiation in natural conditions (fig. S2, A and B). To further explore the effect of PXO99A on *Arabidopsis* reproduction, we performed RNA sequencing (RNA-seq) on wild-type inflorescence apices after infection. The analysis of differentially expressed genes (DEGs) using the Kyoto Encyclopedia of Genes and Genomes (KEGG) and Gene Ontology (GO) illustrated the enrichment in bacterial response pathways and plant hormone signal transduction pathways (Fig. 1I and fig. S3).

To discern how PXO99A directly inhibits ovule initiation, we treated flowers with PXO99A mutants lacking different secretion systems and observed less decreased ovule count in both type III and type VI secretion system (T3SS and T6SS, respectively) mutants, compared to that in the PXO99A (Fig. 1H). This suggests that effectors secreted by these systems inhibit ovule initiation. Notably, the mutant strain lacking the T6SS showed the weakest inhibition, indicating its predominant role in this process. For bacteria, many plant-associated bacteria contain T6SS, which can secrete toxic effectors and gain competitiveness against other bacteria, thus enabling them to obtain a sufficient growth advantage in complex bacterial environments (*19*). The type III system is well-known for infecting host plants (*20*), while the role of the type VI system in such infections has been reported very few (*21*, *22*). We further investigated how the T6SS of PXO99A affects ovule initiation.

PXO99A inhibits ovule initiation by effector TleB

Simultaneous knockout of the putative effectors TleA and TleB from PXO99A (ΔTleA&B), followed by treatment of *Arabidopsis* flowers alongside PXO99A and a mock control, yielded insightful results. Statistical analysis showed that ovule counts in plants treated with PXO99A (ΔTleA&B) were significantly higher than those in plants infected with the wild-type strain but remained slightly lower than those observed in the mock control (Fig. 2, A and C). This outcome suggests that TleA and TleB are the potential effectors responsible for inhibiting ovule initiation in PXO99A. To further confirm the function of these effectors, we designed to overexpress them in wild-type *Arabidopsis*. Given the notable overlap in the amino acid sequences of TleB and TleA, we deduced that their function would be redundant and TleB would be more important; thus, our research focused primarily on TleB for the subsequent experiments [locus numbers: TleA, WP_240321041; and TleB, WP_048488806; both proteins contain Tle1 domain and encode the DUF2235 domain as described in (*23*)]. We overexpressed TleB using the p35S:TleB-GFP vector. Phenotypic analysis of the transgenic plants 35S:TleB-GFP demonstrated that, compared to the wild-type control, these plants exhibited shorter siliques and a similar reduction in seed setting rate as PXO99A treatment (Fig. 2, B and D, and fig. S4), thereby providing clear evidence that TleB directly inhibits ovule initiation.

TleB interacts with PUB14 and is degraded by the 26*S* proteasome

To elucidate the mechanism by which this effector inhibits ovule initiation, we investigated TleB interaction proteins in *Arabidopsis* flowers. Using TleB as bait, we conducted immunoprecipitation coupled with mass spectrometry (IP-MS) using total protein extracts from *Arabidopsis* inflorescence apices and isolated target proteins (fig. S5). Cell-free assays indicated that TleB protein was unstable and underwent degradation in *Arabidopsis* cells, prompting us to focus on candidate proteins involved in protein degradation pathways (Fig. 2E).

Among these candidates, we identified an E3 ubiquitin ligase containing a U-box domain, PUB14 (locus number AT3G54850), which is transcriptionally up-regulated in TleB overexpressing lines and exists in placentae and ovule primordia during ovule initiation stage (Fig. 2, F and G). Structure prediction, co-localization analysis, and bimolecular fluorescence complementation (BiFC) alongside co-immunoprecipitation (co-IP) assays demonstrated that PUB14 interacts with TleB in the cytoplasm of *Arabidopsis* cells (Fig. 2, H to J). The interaction between PUB14 and TleB suggests that TleB may be ubiquitinated and subsequently degraded in plant cells, representing a potential plant response to PXO99A infection. We evaluated the stability of TleB using a cell-free system with the proteasome inhibitor MG132. These results indicate that the reduction of TleB protein was achieved through the 26*S* proteasome, but the 6-hour results indicated that the possibility of other degradation pathways of TleB could not be excluded (Fig. 2K). In vivo ubiquitination assays confirmed that PUB14 can polyubiquitinate TleB, targeting it for degradation via the 26*S* proteasome (Fig. 2L).

PUB14 promotes ovule initiation by stabilizing the positive regulator BZR1

Transcriptome analysis also indicated significant changes in downstream genes of the BES1/BZR1 family compared to other plant hormone transcription factors (TFs) after PXO99A treatment (Fig. 3A). Subsequent Western blot analysis confirmed that BES1 protein levels remained unchanged after PXO99A treatment (fig. S6A); thus, our studies focused on the BZR1 protein. We observed a substantial increase in BZR1 content in inflorescence apices infected with DC3000 and AC, whereas there was a noticeable decrease with PXO99A infection (Fig. 3, B to D, and fig. S6B). These results suggest that PXO99A

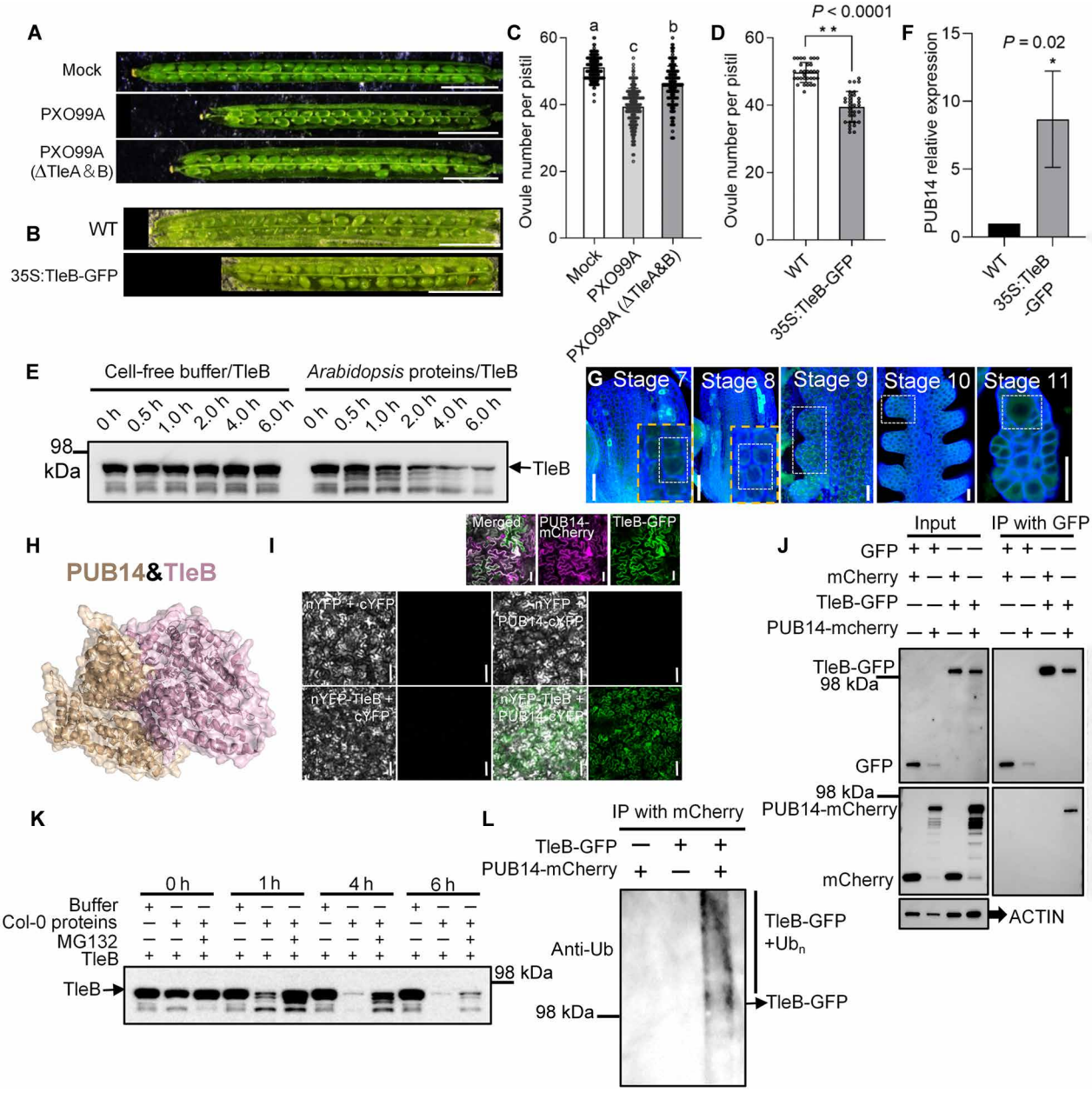

Fig. 2. TleB is ubiquitinated by PUB14 and negatively regulate ovule initiation. (**A** and **C**) Phenotypic and statistical analysis of ovule number per pistil after infection of PXO99A and PXO99A (ΔTleA&TleB). Scale bars, 2 mm. Bars represent means ± SD of three biological replicates ($n = 180$). (**B** and **D**) Phenotypic and statistical analysis of ovule number per pistil of wild type (WT) and 35S:TleB-GFP. Circled are the aborted seeds of failure. Scale bars, 2 mm. Bars represent means ± SD ($n = 30$). (**E**) TleB is unstable in *Arabidopsis* cells (cell-free degradation assay). h, hours. (**F**) Relative expression of PUB14 in 35S:TleB-GFP inflorescence apices. Error bars represent confidence intervals (CIs) calculated using three technical replicates for each sample within the quantitative reverse transcription polymerase chain reaction (qRT-PCR) assay. Asterisks indicate significant differences compared with the respective WT control (Student's *t* test, $*P < 0.05$ and $**P < 0.01$). n.s., not significant. (**G**) Fluorescence observation of pPUB14:PUB14-GFP illustrates that PUB14 expresses in placenta and ovule primordia. Scale bars, 20 μm. Yellow dashed boxes indicate the partially enlarged tissue. White dashed boxes point to the fluorescent signal. (**H**) Prediction structures for PUB14-TleB interaction. (**I** and **J**) PUB14 co-localizes and directly interacts with TleB in plants (BiFC and co-IP in *N. benthamiana*). Scale bars, 100 μm. (**K**) MG132 suppresses TleB degradation in *Arabidopsis* cells (cell-free degradation assay). (**L**) TleB could be ubiquitinated by PUB14.

reduces the stability of BZR1 protein in ovule and TleA and TleB play a key role in this process. The modulation of BZR1 in nonhost plants by bacteria operates independently of the established bacteria resistance pathway in host plants. On the basis of these observations, we hypothesized a functional link between TleB, PUB14, and BZR1. Co-localization studies and BiFC, alongside co-IP assays, demonstrated that PUB14 and BZR1 co-localize and interact with each other during ovule initiation (Fig. 3, E to G, and fig. S7). Further analysis revealed that PUB14 modifies BZR1 probably through mono-ubiquitination (Fig. 3H), a modification playing a crucial role in regulating protein localization and subcellular transport (*24*), unlike polyubiquitination (the typical signals for proteasomal degradation).

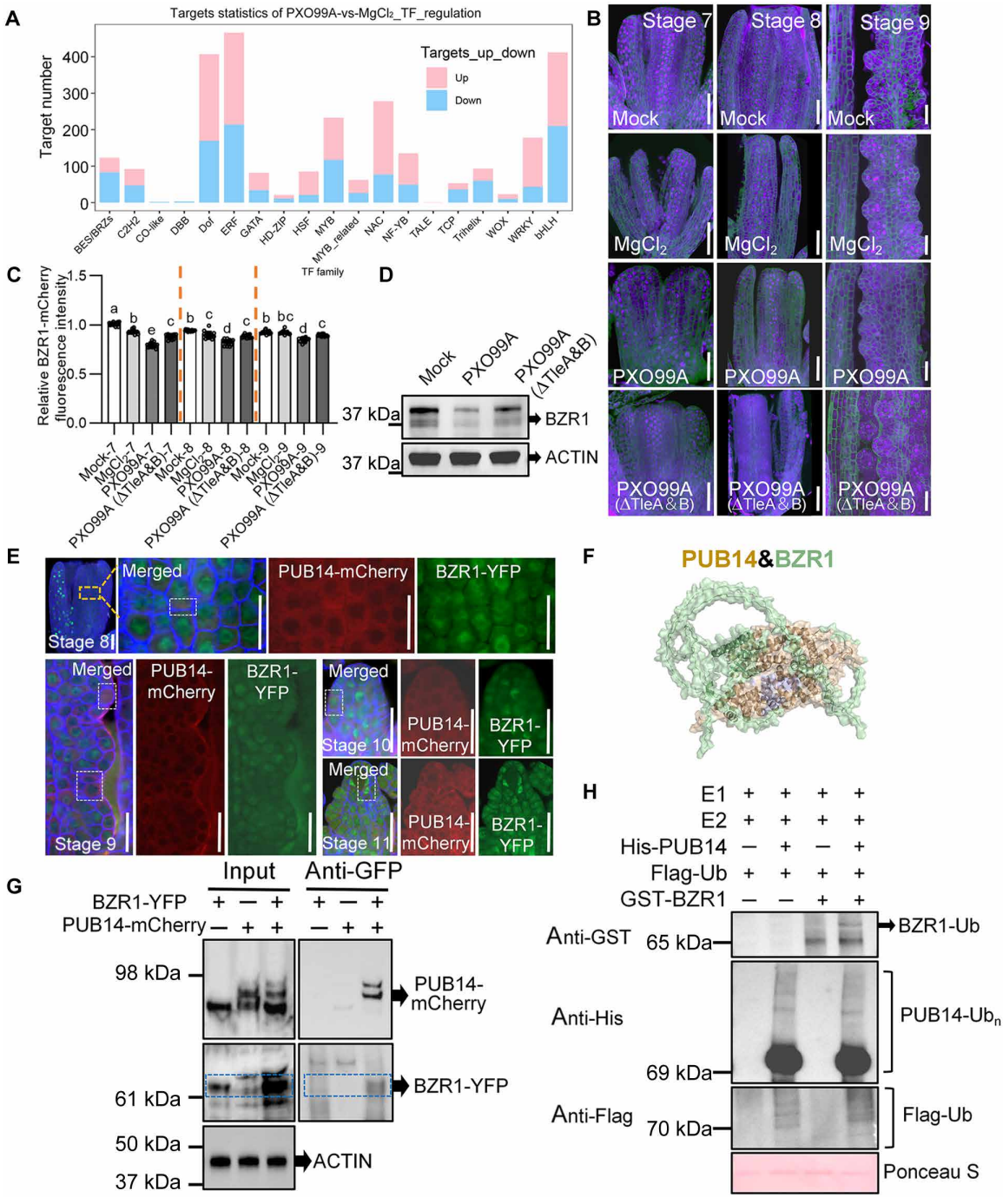

Fig. 3. TleB decreases BZR1 abundance to reduce ovule initiation. (**A**) Bacterial infection transcriptional regulates the expression of BES/BZRs target genes. (**B** to **D**) Bacterial infection decreases BZR1 abundance in placenta and ovule primordia. Scale bars, 20 μm. Lowercase letters indicate significant differences among different stages (one-way ANOVA, $P < 0.05$) ($n = 15$). (**E**) PUB14 and BZR1 co-localize in placenta and ovule primordia. Scale bars, 20 μm. Yellow dashed boxes indicate the partially enlarged tissue. White dashed boxes point to the fluorescent signal. (**F**) Prediction structures for PUB14-BZR1 interaction. Purple region represents the area where interactions are taking place. (**G**) PUB14 interacts with BZR1 directly. The dashed box circles the bands. (**H**) BZR1 could be mono-ubiquitinated by PUB14.

To further investigate the role of PUB14, we generated transgenic plants overexpressing PUB14 under the UBQ10 promoter (UBQ10:PUB14-mCherry) and observed an increase in silique length and a 15 to 18% increase in ovule number per pistil compared to that in the wild type (Fig. 4, A to C, and fig. S5). Transferred DNA (T-DNA) insertion line *pub14-2* (SALK_059924C) with elevated PUB14 expression (fig. S8, A and B) also exhibited a 15% increase in seed number per silique, similar to UBQ10:PUB14-mCherry, and displayed increased insensitivity to PXO99A infection concerning ovule number (fig. S8C). Meanwhile, we constructed two CRISPR lines of PUB14 named *PUB14 CRISPR* and *PUB14 CRISPR2*. These two lines have the similar phenotype, the amino acids were terminated earlier after the mutation, and the seed number was significantly decreased compared with that in the wild type (fig. S8, A and D). Thus, the subsequent experiments were conducted using the *PUB14 CRISPR* line. The statistics of the ovule number revealed that *PUB14 CRISPR* resulted in a 20% decrease in ovule number per pistil, further substantiating the role of PUB14 in enhancing ovule initiation and seed production (Fig. 4, A to C, and fig. S8D). In addition, Western blot analysis revealed that, compared with the wild type, there were no normal sized PUB14 in the PUB14 genome editing line *PUB14 CRISPR*, and the BZR1 protein level was notably reduced. In the PUB14 overexpression line UBQ10:PUB14-mCherry, the protein level of PUB14 and BZR1 increased (Fig. 4, D and E). These results confirm that PUB14 positively regulates BZR1 protein levels, thereby promoting ovule initiation. We performed the transcriptome analysis of *PUB14 CRISPR* and overexpression line UBQ10:PUB14-mCherry. DEGs revealed that the expression of ovule initiation-related

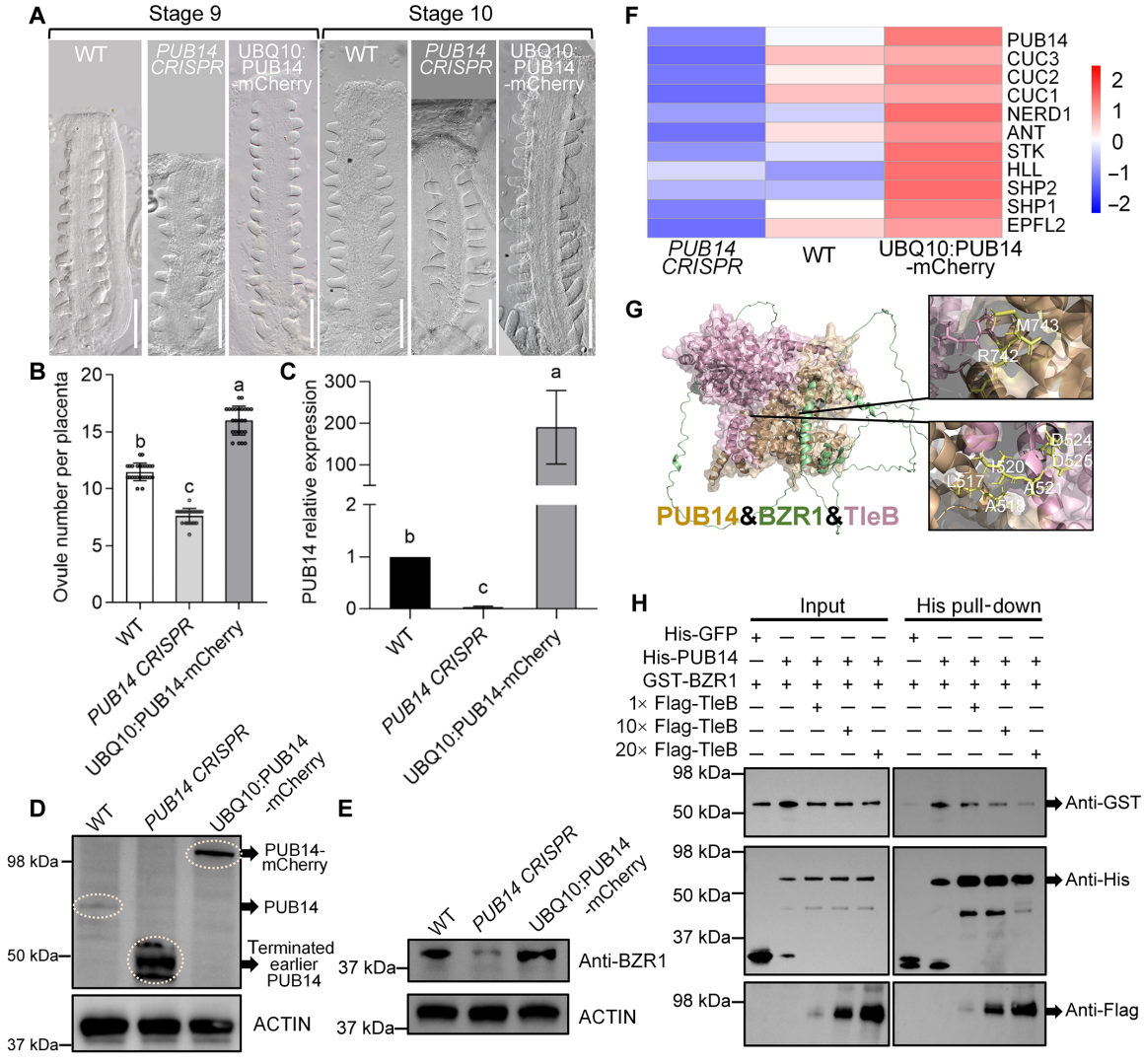

Fig. 4. TIeB inhibits the interaction of PUB14 and BZR1 and suppresses ovule initiation through competitive combining with PUB14. (**A** and **B**) Phenotypic and statistical analysis of ovule number per placenta in WT, UBQ10:PUB14-mCherry, and *PUB14 CRISPR*. Bars represent means ± SD ($n = 25$). Scale bars, 100 μm. (**C**) Relative expression of PUB14 in the inflorescence apices of WT, UBQ10:PUB14-mCherry, and *PUB14 CRISPR* lines. Error bars represent CIs calculated using three technical replicates for each sample within the qRT-PCR assay. (**D**) Protein level of PUB14 in the inflorescence apices of WT, *PUB14 CRISPR*, and UBQ10:PUB14-mCherry lines. (**E**) PUB14 positive regulates BZR1 abundance in inflorescence apices. (**F**) DEGs related to ovule initiation in the inflorescence apices of WT, UBQ10:PUB14-mCherry, and *PUB14 CRISPR* lines. (**G**) Prediction structures for PUB14-BZR1-TIeB interaction. The enlarged image shows the key sites of the PUB14-TIeB interactions. (**H**) TIeB inhibits PUB14-BZR1 interaction through competitive combining with PUB14. Lowercase letters indicate significant differences among different stages (one-way ANOVA, $P < 0.05$).

genes was reduced in *PUB14 CRISPR* and significantly increased in UBQ10:PUB14-mCherry compared to that in the wild type (Fig. 4F). The above results are also consistent with the increased ovule number in UBQ10:PUB14-mCherry plants.

Previous research has documented the coevolution of pathogens and plants, which co-regulate plant defense responses to pathogens. To address whether there are similar mechanisms mentioned above in other species, we performed an evolutionary analysis of the PUB14 and BZR1. Phylogenic analysis revealed that they exist in many plants (fig. S9), including *Brassica napus* L., *Solanum lycopersicum* L., and *Petunia hybrida*. The results indicated that the effector inhibition to the interaction of PUB14 and BZR1, leading to repressed ovule initiation and decreased seed number, may exist in different nonhost species. As expected, we got similar phenotypes in other nonhost plants after bacterial infection, such as rapeseed, tomato, and petunia (fig. S10). In some monocotyledons, predictions indicated that effector from DC3000 (non-adapted pathogen for rice, maize, and wheat) also inhibits the interaction of their PUB14-BZR1 modules, suggesting that the mechanism broadly generalized across species (fig. S11).

TleB inhibits the interaction of PUB14 and BZR1 and suppresses ovule initiation through competitive binding with PUB14

Although PUB14 stabilizes BZR1 and enhances ovule initiation, the induction of PUB14 in response to TleB does not promote and may even inhibit ovule initiation (Fig. 2, B, D, and E). The interaction between PUB14 and BZR1, when induced by PXO99A, differs from that observed with normal PUB14 overexpression, suggesting a competitive interaction (Figs. 3G and 5A). We hypothesized that BZR1 is suppressed during PXO99A infection despite the increase in PUB14. TleB likely disrupts the interaction between PUB14 and BZR1 by competitively binding to PUB14, thereby inhibiting ovule initiation.

To test this hypothesis, we used AlphaFold2 (multimer v3) to predict the protein structures of TleB with PUB14, PUB14 with BZR1, and all three proteins together (*25*). The predictions confirm that PUB14 can bind to both TleB and BZR1 (consistent with experimental observations) (Fig. 4G). Detailed structural analysis indicated that the protruding C-terminal domain of TleB fits well into the funnel-like structure of PUB14. The interaction between PUB14 and BZR1 is similar yet weaker than that between PUB14 and TleB. Notably, the presence of TleB reduces the interaction between PUB14 and BZR1, as TleB occupies the binding sites on PUB14 that interact with BZR1, suggesting that TleB competitively inhibits this interaction, leading to decreased levels of BZR1, which would, otherwise, be stabilized by PUB14. To validate this competitive interaction, we expressed and purified PUB14-His, BZR1–glutathione *S*-transferase (GST), and TleB-FLAG proteins in vitro. Pull-down assays demonstrated that, while PUB14 binds to BZR1, this interaction weakens with the addition of TleB. As the concentration of TleB increases, the interaction between PUB14 and BZR1 correspondingly decreases (Fig. 4H), confirming that TleB competitively interacts with PUB14, thereby disrupting its interaction with BZR1. Structural predictions further identified potential binding regions of PUB14 with TleB and BZR1. We mutated the overlapping binding sites on TleB and conducted in vitro competitive binding experiments with the mutated TleB protein. These experiments showed that the mutated TleB disrupted the interaction between PUB14 and BZR1 at a much less level compared to the original TleB (Fig. 5A). Furthermore, treating *Arabidopsis* flowers with PXO99A containing the mutated TleB protein did not lead to as severe a decrease in BZR1 protein levels and ovule number as observed with the PXO99A (Fig. 5, B and C), reinforcing that TleB competitively inhibits the interaction between PUB14 and BZR1, thereby suppressing ovule initiation and reducing seed number.

In summary, our study elucidates how the PXO99A suppresses ovule initiation and reduces seed number in nonhost plant *Arabidopsis* without causing overt disease. In the absence of bacterial infection, PUB14 interacts with and stabilizes BZR1 to promote ovule initiation. The primary effector TleB disrupts this interaction between PUB14 and BZR1, leading to decreased BZR1 levels and reduced ovule numbers. PUB14 ubiquitinates TleB, targeting it for its degradation via the 26*S* proteasome. These findings highlight that bacterial infection to nonhost plants during reproductive development leads to the standby status, and PUB14 potentially mediates the trade-off between reproduction and defense (Fig. 5D).

DISCUSSION

In nature, different types of plants often grow closely together; roots or branches from different plants can interweave; and bacteria can be transmitted from one plant to another via wind, pollen, seeds, or insects. In our greenhouse, we detected bacteria on common flying insects such as aphids and thrips. Metagenomic data identified various bacteria on these insects, indicating that different bacteria might shuttle between host and nonhost plants (fig. S2) and bacteria can settle on nonhost plants, including flowers, in natural conditions.

Previous studies have primarily focused on how pathogens infect plant vegetative organs, such as leaves, to understand their impact on plant growth and development (*26*). Researchers often measure lesion size and, occasionally, seed yield to assess pathogen impact (*7*). It is well-documented that pathogen infection during vegetative growth inhibits plant growth and negatively affects reproductive development, leading to decreased seed quantity and quality. However, there is limited research on the regulatory mechanisms by which biotic stress directly affects reproductive development and seed formation (*27*, *28*). Plant reproductive growth is a critical stage and highly sensitive to environmental conditions. PXO99A infection leads to repressed ovule initiation and reduced ovule number, as well as aborted seeds, suggesting that bacteria also disturb the seed development. We focus on ovule initiation in this study. Our previous work demonstrated that ovules do not initiate simultaneously but in two to three rounds (*8*, *9*), suggesting that ovule initiation could be adjusted on the basis of environmental conditions. This study further demonstrates that an unfavorable environment reduces seed numbers by suppressing ovule initiation. Our research reveals the direct impact of bacterial infection on the reproduction of nonhost plants. Because this bacterial infection does not induce lesions, it could be considered an environmental signal regulating plant reproductive development, representing a regulatory mechanism. This study expands our understanding of plant-pathogen interactions, highlighting the need to consider biotic stresses in reproductive development studies.

Bacteria mainly infect plant growth and development by secreting effectors through specialized secretion systems (*29*). The T3SS is well-known for its role in infecting plants (*20*). The T6SS also secretes effectors, but it is generally known for targeting competing bacterial cells to gain a competitive advantage (*19*, *30*). In addition,

T6SS has been reported to affect signaling pathways in animal cells (*31*). Our study demonstrates that the T6SS effectors TleA and TleB directly influence plant reproductive development, representing a substantial discovery in understanding bacterial-plant interactions.

PXO99A, a non-adapted bacterium for *Arabidopsis*, does not cause disease in vegetative organs but inhibits ovule initiation and decreases seed number when infecting reproductive organs. PXO99A encodes two distinct T6SSs. On the basis of our results (Fig. 2, A to D), we chose TleA and TleB (identified as effector proteins of T6SS-2, members of the Tle1 family) for this study (*23*). However, we do not exclude that other effectors also have regulatory roles in ovule initiation under biotic stress. This part deserves further exploration.

We analyzed the transcriptome of young flowers treated with PXO99A, including mock control, PXO99A, and PXO99A (ΔTleA&B) treatments. GO analysis of PXO99A treatment identified DEGs enriched in salicylic acid and jasmonic acid signaling, hydrogen peroxide metabolism, bacterial response, glutathione metabolism, toxin degradation metabolism, oxidative stress response, chitin response, and chitinase activity regulation pathways. These responses are similar to general plant responses to bacterial infection. KEGG enrichment analysis revealed that DEGs were mainly enriched in plant hormone signaling pathways and mitogen-activated protein kinase (MAPK) signaling pathways. Key genes in plant hormone signaling pathways, including AUX/IAA (auxin-related), EIN3 (ethylene-related), BZR1and BES1 (BR-related), and PR1 (CK-related), were down-regulated, while key genes in the MAPK signaling pathway, such as RbohD and OXI1, were up-regulated. Although no disease induced, PXO99A treatment in flowers induces disease resistance–related genes while repressing growth-related genes, consistent with plant resistance responses to bacterial infection. The data suggest that bacterial infection can shift the priority of nonhost plants from growth to the standby status, being ready to disease resistance. The induction of PTI in *Arabidopsis* indicated that the plant can undergone a defense response anytime if needed. The decrease in seed number might be a compromise of *Arabidopsis* with the bacterial environment. The reduced seed number stored nutrients in the plant body, such as vascular bundles and intercellular spaces, while PXO99A could use these nutrients for survival, thereby reducing the adverse effects on the formed seeds.

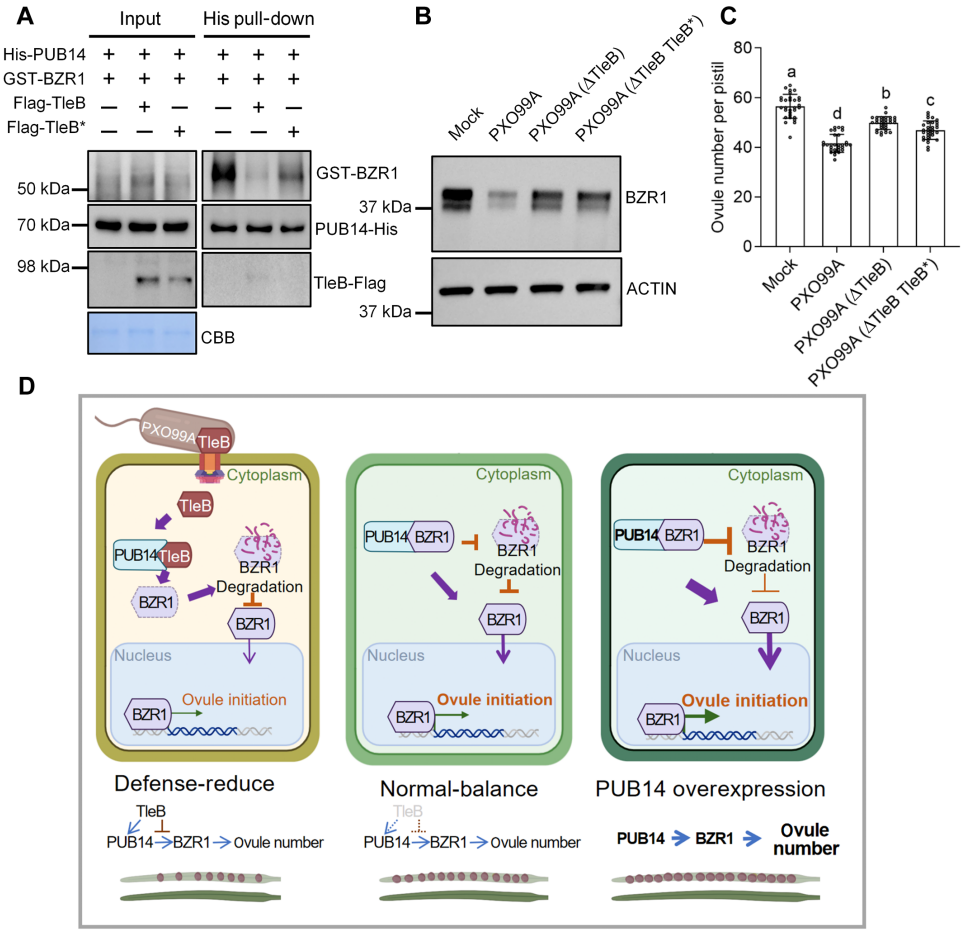

Fig. 5. Mutation in the binding sites of TleB with PUB 14 decreases TleB inhibition of the interaction of PUB 14 and BZR1. (**A**) TleB* also inhibits the interaction of PUB14 and BZR1 through competitive combining with PUB14, but the inhibition of TleB* is lower than that of TleB (* represent mutations at key sites in Fig. 4G, * represents 516 to 525 amino acids to A, and 727 to 743 amino acids to A in TleB). (**B**) The degree of PXO99A (ΔTleB TleB*)'s infection decreasing BZR1 abundance is lower than that of PXO99A. (**C**) The degree of PXO99A (ΔTleB TleB*)'s infection decreasing ovule initiation is lower than that of PXO99A. Bars represent means ± SD ($n = 30$). (**D**) Work model of TleB-PUB14-BZR1 module–related reproduction-defense trade-off. Lowercase letters indicate significant differences among different stages (one-way ANOVA, $P < 0.05$).

In addition, BZR1, a key factor promoting ovule initiation, was down-regulated at the transcription level, which may contribute to the decreased BZR1 protein level, providing another mechanism for the reduced ovule initiation observed with PXO99A treatment. Previous reports demonstrated that PUB40 could ubiquitinate BZR1 and promote BZR1 degradation (*32*). Our experiments indicated that PUB14 probably competitively inhibited the binding of PUB40 to BZR1, further implying that PUB14 promotes protein stabilities of BZR1 (fig. S12).

The phenotypes vary notably when different bacteria (AC, DC3000, and PXO99A) infect *Arabidopsis* flowers. Bacteria cause flowers to wilt and produce no seeds in the host plant, while these result in normal flower development but decreased seed set in the nonhost plant. This suggests that, for nonhost *Arabidopsis*, bacteria act more as environmental signals than pathogens. For instance, while AC and PXO99A are not host-adapted bacteria of *Arabidopsis*, AC infection causes damage to flower organs and even leads to wilted flowers. This could be because the host plant of AC (which primarily infects cucumis melon) is closer to *Arabidopsis* than PXO99A (which primarily infects rice) (fig. S1B) (*33*, *34*). When we reduced the titer and treatment time of AC, the flowers did not wilt, but the seed set decreased, similar to the PXO99A treatment. These results suggest that bacterial infection activates a plant defense response and induces general disease resistance without causing severe pathological symptoms or hypersensitive reactions in nonhost plants. Non-adapted pathogens act as unfriendly environmental signals (*17*), which can disturb plant development, particularly reproduction if they accumulate or invade critical tissues (*35*), rather than cause disease or death. Bacterial invasion of flowers of nonhost plants reduces seed set, likely as a strategy to ensure the development of existing ovules and the survival of plants and developing seeds. Therefore, if bacteria are to be used as biological pesticides or biocontrol agents for nonhost plants, then these side effects should be carefully managed.

The results demonstrate that the T6SS can directly influence plants, sometimes even more than the T3SS, which is known for causing host diseases. Notably, T6SS is active during non-adapted pathogen infections. When we treated other dicot plants, such as tomato, with PXO99A, it also affected the seed set. These findings indicate that the infection of reproductive organs by non-adapted pathogens can generally influence seed formation. PXO99A infection leads to increased PUB14 expression in *Arabidopsis*, quantitative reverse transcription polymerase chain reaction (qRT-PCR) analyses showed that PUB14 transcription levels significantly increased 6 hours after infection with both PXO99A and PXO99A (ΔTleA&B) strains (fig. S13A). Western blot analyses further confirmed an increase in PUB14 protein levels following infection (fig. S13B). These results suggest that PXO99A (ΔTleA&B) could potentially be used as a vaccine to enhance *Arabidopsis* resistance.

The T6SS in plant-associated bacteria can secrete toxic effector proteins, increasing bacterial competitiveness and allowing them to obtain more nutrients and space from plants (*36*–*38*). On the basis of our results (fig. S14), we hypothesize that the effector TleB secreted by T6SS competitively inhibits the binding of PUB14 and BZR1 in both host and nonhost plants, leading to reduced seed numbers to gain more nutrients. This process might be overshadowed by a more vigorous immune response in host plants. In nonhost plants, the disruption of the PUB14-BZR1 interaction results in more TleB being ubiquitinated and degraded (Fig. 2K), reducing the impact of bacterial infections (fig. S8C). BAK1-BKK1 pathway mutant *bak1bkk1*, displayed deficient in PTI, have similar reduced seed numbers after PXO99A infections compared to wild type (fig. S8C); therefore, the effect of PUB14 on the seed number after bacterial infection is independent of the PTI pathway. At the same time, the reduced seed number conserves nutrients during reproduction, helping the plant resist various pathogens. This phenomenon and regulatory mechanism, existing in many plants, indicate an interaction between bacteria and plants during evolution (*36*). The reported other U-box domain–containing E3 ubiquitin ligases function in the trade-off of immune response and plant development (*39*), while the signaling pathways involved in trade-off have been extensively studied in vegetative stages (*40*). Our work imply a kind of balance between growth and defense during reproductive development.

In summary, we identified a key gene, PUB14, being responsible for the trade-off between reproduction and defense in plant. The suppressed reproduction makes plant standby under the unfriendly environments with bacteria. We demonstrated that TleB, the effector of the T6SS in bacteria, can competitively inhibit the interaction between PUB14 and BZR1 in nonhost plants, thereby suppressing ovule initiation and reducing seed number; our findings indicate that plants adjust their offspring number based on environmental signals to ensure the survival and quality of their progeny.

MATERIALS AND METHODS

Plant materials and growth conditions

The *Arabidopsis* plant materials in this research were in the Col-0 [wild-type, *Arabidopsis thaliana* (L.) *Heynh*] ecotype background. The plants used in this study including *pub14-2* (SALK_059924C), *bak1bkk1* (provided by G. Yu), pBZR1:BZR1-YFP (provided by W.-Q. Tang) (*41*), and pBZR1:BZR1-mCherry were described in previous studies (*42*). The 35S:TleB-GFP, UBQ10:PUB14-mCherry, and pPUB14:PUB14-GFP vectors were transformed into wild-type *Arabidopsis* plants. *Agrobacterium*-mediated transformation was performed using the floral dip method (*43*).

Following procedures previously described in (*42*), seeds were sterilized with 2% NaClO for 5 min, washed three times with sterile water, and then placed on half-strength Murashige and Skoog ($^1/_2$ MS) medium containing 1.5% sucrose and 0.75% agar (pH 5.7) (*44*). After a 2-day vernalization at 4°C, the seeds were placed in a growth chamber for 7 days. Then, the seedlings were transferred to soil and grown at the stable growth conditions: temperature at 22°C and a 16-hour light–8-hour dark cycle.

Strains and growth conditions

All strains and plasmids used in this study are listed in the extended data. PXO99A was cultured in nutrient broth (NB) medium (0.3% beef extract, 0.1% yeast extract, 0.5% polypeptone, and 0.5% sucrose) under aerobic conditions at 28°C. The strain mutants including PXO99A (ΔT3SS, ΔT6SS, ΔT3, 6SS, TleA&B, and TleB) were constructed on the basis of the suicide plasmid pK18mobSacB using homologous double exchange, and all constructs were verified through sequencing (*45*).

Plasmid construction, plant transformation, and identification

To generate the pPUB14:PUB14-GFP construct, the promoter and genomic DNA fragments of PUB14 were amplified by PCR using genomic DNA of wild type as templates and then cloned into the pHB vectors (Biovector NTCC) digested by Eco RI and Hind III.

To generate the UBQ10:PUB14-mCherry construct, we first modified the pHB vector by replacing the 2× 35*S* promoter with a UBQ10 promoter. Then, we cloned the full-length coding sequence of PUB14 into the Bam HI sites of the modified pHB vector.

To generate the 35S:TleB-GFP construct, we cloned the full-length coding sequence of TleB from the PXO99A into the Bam HI sites of the modified pHB vector.

To generate the His-PUB14 and His-TleB constructs, we cloned the full-length coding sequence of PUB14 into the Bam HI sites of pET-28a(+) (New England Biolabs).

To generate the Flag-TleB construct, we cloned the full-length coding sequence of TleB into pBBR1MCSArac vector by Gibson Assembly (New England Biolabs).

To generate the Flag-TleB* (* represents 516 to 525 amino acids to A, and 727 to 743 amino acids to A in TleB) construct, we cloned the full-length coding sequence of TleB and introduced mutation sites using the Fast Mutagenesis System (FM111-01, TransGen Biotech) according to the manufacturer's instructions.

To generate the MBP-PUB40 construct, the full-length coding sequence of PUB40 was cloned into pMal-c2X (New England Biolabs). GST-BZR1 construct based on pET-GST was described in our previous study (*15*).

Following procedures previously described in (*42*), to generate the constructs related to BiFC assays, the full-length coding sequences of TleB, PUB14, and BZR1 were cloned into the Bam HI site of vectors pXY104 and pXY106, encoding the C- and N-terminal halves of yellow fluorescent protein (YFP; cYFP and nYFP), respectively.

For the *PUB14 CRISPR* construct, two 19–base pair (bp) fragments of the PUB14 coding sequence (GATATCACTTGAACTGATGA and AAAGGAGCCATTGTTGATGC) were chosen. Using the pCBC-DT1T2 plasmid as a template, a fragment was amplified using primers containing the above two segments, which was ligated into the pHSE401 plasmid as reported (*46*).

Following experimental procedures previously described in (*42*), to generate transgenic plants, the corresponding constructs were transformed into *Agrobacterium tumefaciens* (strain GV3101) and then into wild type by the floral dip method (*43*). Primers used to generate the abovementioned constructs are listed in table S1, and all constructs were confirmed by sequencing and alignment before being used in transformation. Transgenic plants were selected on $^1/_2$ MS medium containing specific antibiotics, and the homozygous transgenic plants were used in further assays.

The *pub14* mutant, T-DNA insertion line *pub14-2* (SALK_059924C), was ordered from the ARASHARE (www.arashare.cn/index/). Primers for genotyping of the T-DNA insertion lines are listed in table S1.

Confocal microscopy

Following procedures previously described in (*42*), samples were observed with an Upright Laser Confocal Microscope (Nikon & Nikon Ni-E A1 HD25). The excitation and emission wavelengths were as follows: green fluorescent protein (GFP) and YFP, excitation at 488 nm and emission at 505 to 550 nm; and mCherry, excitation at 561 nm and emission at 575 to 620 nm. All samples were observed using the same parameters: confocal pinhole, 1.2 μm; excitation intensity, 5; and high voltage (HV), 30 (*42*).

Infection assay

To infect live *A. thaliana* inflorescence apices, a 200-μl PCR tube was inverted on a stick, and 50 μl of bacterial solution was added (*16*). The bacterial solution was prepared by resuspending bacteria in a 10 mM $MgCl_2$ solution containing 0.1% Triton X-100 (Sigma-Aldrich, T9284) and had an OD_{600} of 0.8. Before infection, older flowers with fertilized ovules were removed. The top of the *Arabidopsis* inflorescence apices was then immersed in the bacterial solution for 3 hours. After the incubation, the PCR tube containing the solution was removed, and the plants were cultured under normal environmental conditions (20° to 22°C, 16 hours of light, and 8 hours of darkness). Subsequently, materials for fluorescence observation were taken at 6 hours after infection, and materials for DIC microscope of ovule initiation were taken at 24 hours after infection. The total number of seeds in six to eight mature siliques was counted after 7 to 10 days of culture for further analysis.

Metagenomic sequencing

Insect samples were collected from greenhouses. The sample was mixed and placed in a 1.5-ml centrifuge tube, and DNA was extracted using the cetyltrimethylammonium bromide (CTAB) method (*47*). The genomic DNA sample was fragmented into short fragments with the length of ~350 bp. After randomly breaking fragments with a length of about 350 bp using a Covaris ultrasonic crusher, the library was constructed. The entire library was prepared through steps such as end repair, addition of A-tail, addition of sequencing adapters, purification, and PCR amplification. The raw data were obtained through Illumina PE150 sequencing in the library. Fastp (https://github.com/OpenGene/fastp) was used for preprocessing raw data from the Illumina sequencing platform to obtain clean data for subsequent analysis (*48*). Considering the presence of host contamination in samples, Bowtie2 (http://bowtie-bio.sourceforge.net/bowtie2/index.shtml) was used to filter out reads that may originate from host (*49*), including *Sitobion avenae*, *Lipaphis erysimi*, *Nilaparvata lugens*, *Stenchaetothrips biformis*, *Franjliniella occidentalis*, and *A. thaliana*. MEGAHIT software was used for assembly analysis of clean data, and MetaGeneMark (http://topaz.gatech.edu/GeneMark/) and CD-HIT software (www.bioinformatics.org/cd-hit/) were used to obtain the nonredundant initial gene catalogue (*50*, *51*). Bowtie2 was used to compare the clean data of each sample with the initial gene catalogue, the number of gene reads on each sample comparison was calculated, and the gene abundance was lastly determined for Krona analysis (*20*). Raw data have been uploaded in the Supplementary Materials and DRYAD database (https://doi.org/10.5061/dryad.jwstqjqkp).

Phenotypic and statistical analysis of ovule initiation

For DIC observations, pistils were dissected from fresh flowers at stages 8 to 12 under a stereoscope microscope and then were placed in a drop of chloral hydrate solution (chloral hydrate:H_2O:glycerol, 8:3:1) until the pistils cleared. Cleared pistils were observed under a microscope (Zeiss Axio Imager M2) with DIC optics.

For statistics of ovule number, we took the vigorously growing buds from outside to inside of inflorescence apices. For the analysis of flowers containing GFP or mCherry constructs, we first carefully peeled the pistils from the flowers in different treatment conditions and fixed them in 4% paraformaldehyde for 30 min and then immersed in ClearSee agent according to ClearSee method (*52*). Before observation, materials were soaked in ClearSee reagent to wash away the cell wall stain (FB28) for more than half an hour. For the ovule wrapped inside the pistils, we tapped the corresponding position of the coverslip with the tip of the tweezers to expose the ovule. Then, we used the Upright Laser Confocal Microscope (Nikon & Nikon Ni-E A1 HD25) for observation and photography.

Cell-free assay

For cell-free assay, 0.1 g of inflorescence apices were immersed in liquid nitrogen immediately and grounded into powders using multi-sample freeze grinder (Wonbio-Mini). The pellet of inflorescence was resuspended in lysis buffer [25 mM tris-HCl (pH 7.5), 10 mM NaCl, 10 mM $MgCl_2$, 5 mM dithiothreitol (DTT), 0.4 mM phenylmethylsulfonyl fluoride, and 10 mM adenosine 5′-triphosphate (ATP)] and lysed on ice for 30 min. Next, 1 μg of His-TleB recombinant protein was incubated with individual extracts in darkness at 22°C for specific time periods, and the proteasome inhibitor MG132 was added to the experimental group. The samples were mixed with loading buffer and boiled at 100°C for 10 min followed by SDS–polyacrylamide gel electrophoresis (PAGE). The anti-His antibody (Abways, catalog no. AB0029; 1:3000 dilution) was used to analyze protein degradation (*53*).

IP-MS assay

The 2 μM His-TleB protein was mixed with the supernatant of *Arabidopsis* inflorescence apices using the same method as cell-free assay above. The system was eluted with 2× SDS loading buffer and immediately boiled for 15 min. The input and eluted proteins were separated by 4 to 20% Precast PAGE Gel (ACE Biotechnology) and then subjected to Coomassie blue staining.

The MS analysis was performed as previously described (*54*). Protein bands on the SDS-PAGE gel were destained and then reduced in 10 mM of DTT at 56°C for 30 min followed by alkylation in 55 mM of iodoacetamide at dark for 1 hour. After that, the protein bands were in-gel digested with sequencing-grade trypsin [trypsin (10 ng/μl) and 50 mM of ammonium bicarbonate at pH 8.0] overnight at 37°C. Peptides were extracted with 5% (v/v) formic acid/50% (v/v) acetonitrile and 0.1% formic acid/75% acetonitrile sequentially and then concentrated to 20 μl. Mobile phase A (100% water and 0.1% formic acid) and B solution (80% acetonitrile and 0.1% formic acid) were prepared. The lyophilized powder was dissolved in 10 μl of solution A, centrifuged at 14,000*g* for 20 min at 4°C, and 1 μg of sample was injected into EASY-nLCTM 1200 nano-upgraded ultra high performance liquid chromatography (UHPLE) system with a homemade C18 Nano-Trap column (4.5 cm by 75 μm, 3 μm). Peptides were separated in a homemade analytical column (15 cm by 150 μm, 1.9 μm), using a linear gradient elution. The separated peptides were analyzed by Q Exactive HF-X mass spectrometer, with ion source of Nanospray Flex (electrospray ionization), spray voltage of 2.1 kV, and ion transport capillary temperature of 320°C. Full scan ranges from mass/charge ratio (*m*/*z*) 350 to 1500 with resolution of 60,000 (at *m*/*z* 200), an automatic gain control (AGC) target value was 3×10^6, and a maximum ion injection time was 20 ms. The top 40 precursors of the highest abundance in the full scan were selected and fragmented by higher-energy collisional dissociation and analyzed in MS/MS, where resolution was 15,000 (at *m*/*z* 200), the AGC target value was 1×10^5, the maximum ion injection time was 45 ms, the normalized collision energy was 27%, the intensity threshold was 2.2×10^4, and the dynamic exclusion parameter was 20 s. The raw data of MS detection were named ".raw." The resulting spectra from each fraction were searched separately against UniProt database by the search engines: Proteome Discoverer. The search parameters are set as follows: mass tolerance for precursor ion was 10 ppm, and mass tolerance for product ion was 0.02 Da. Carbamidomethyl was specified as fixed modifications, oxidation of methionine (M) was specified as dynamic modification, and loss of methionine was specified at the N terminus. A maximum of two missed cleavage sites were allowed. To improve the results quality, the software PD further filtered the retrieval results: Peptide spectrum matches (PSMs) with a credibility of over 99% were identified. The identified protein contains at least one unique peptide. The identified PSMs and protein were retained and performed with false discovery rate under 1.0%.

Ubiquitination assay

For in vitro ubiquitination assay, we prepared a 40 μl [10× 4 μl of reaction buffer, 4 μl of E1 enzyme (0.5 μg/μl), 8 μl of ubiquitin solution (1 mg/μl), 10× 4 μl of Mg^{2+}-ATP solution, 4 μl of E2 enzyme (1 μg/μl), and 2 μM purified E3 ubiquitin ligase PUB14 protein, in which the total volume was supplemented to 40 μl with ddH_2O; reagents ordered from UB biotech corporation] of the system on a shaker at 30°C for 1 hour at 900 rpm. Then, the samples were mixed with loading buffer and boiled at 100°C for 10 min, and followed by SDS-PAGE.

For in vivo ubiquitination assay, we conducted co-IP assay for *Nicotiana benthamiana* leaves harboring UBQ10:PUB14-mCherry and 35S:TleB-GFP. Then, we detected the ubiquitination level of TleB using Ubi antibody in Western blot analysis.

Scanning electron microscopy

After infecting *Arabidopsis* inflorescence apices with bacteria for 3 hours, the inflorescence apices were dissected following 24 hours of light culture. The pistils were promptly immersed in 4% glutaraldehyde, subjected to a 10-min vacuum treatment, and then washed five times with 1× phosphate-buffered saline (PBS) buffer for 5 min each. Subsequently, the samples were dehydrated using a gradient of ethanol (45, 55, 70, 85, 95, 100, and 100%). The dehydrated samples were then subjected to carbon dioxide critical point drying, followed by gold spraying, and lastly observed using a scanning electron microscope.

RNA extraction and qRT-PCR analysis

The materials used for total RNA extraction in this study were inflorescence apices of *Arabidopsis*, which were harvested with tweezers and quick-frozen in liquid nitrogen. Subsequent RNA extraction and reverse transcription were performed using the RNAprep Pure Plant Kit (TIANGEN) and the RevertAid First Strand cDNA Synthesis Kit (Thermo Fisher Scientific) following the manufacturers' protocols. qRT-PCR assays were conducted for three technical replicates of three biological replicates, and the results are shown as the means ± SDs. The details were carried out as described previously (*55*). Results were normalized using ACTIN2 as the endogenous control. The sequences of oligonucleotide primer sets used are listed in table S1.

Western blot analysis

Total proteins were extracted using 2× SDS buffer containing 0.5 M tris-HCl (pH 6.8), 3% DTT, 4% (w/v) SDS, 20% (v/v) glycerol, and 0.2% (w/v) bromophenol blue. Then, the protein samples were placed in the boiling water for 10 min followed by cooling. The mixture of proteins was separated on 4 to 20% Precast PAGE Gel (ACE Biotechnology) and subsequently transferred onto a polyvinylidene fluoride membrane (Whatman, Buckinghamshire, UK). The membranes were incubated with the first antibodies anti-BZR1 (1:3000, Youke Biotech), anti-BES1 (1:3000, PhytoAB), anti-GFP (1:5000, Abways), anti-mCherry (1:5000, Proteintech), anti-PUB14 (1:1000, Orizymes), anti-Ubi (1:3000,

Abcam), anti-Flag (1:3000, Smart-Lifesciences), anti-His (1:3000, Smart-Lifesciences), anti-GST (1:3000, Abways), anti-MBP (1:3000, Abways), and internal control ACTIN (1:3000, ABclonal), respectively, overnight at 4°C after blocking with 5% skim milk. The blocked membranes were washed three times by PBS with Tween 20 (PBST) each step for 10 min. Then, the membranes were incubated with the secondary antibody goat antirabbit or goat antimouse immunoglobulin G with horseradish peroxidase–conjugated (1:5000, Sharebio) for 3 hours at room temperature and washed three times with PBST. The signals were illustrated by enhanced chemiluminescence (ECL) solutions (Sharebio) for 5 min in the darkness and were photographed by Bio-Rad machine with a charge-coupled device camera system.

In vitro pull-down assays

For in vitro pull-down assays, proteins were expressed and purified in *E. coli* (strain BL21) as described in (*15*). According to experimental procedure described in (*42*), 3 μg of purified recombinant bait proteins and 5 μg of prey proteins were added to 1 ml of binding buffer with 200 μl of GST/His agarose beads (Smart-Lifesciences) (prepared as instructions on the official website of Smart-Lifesciences). After incubation at 4°C for 1 hour, samples were washed three times with the washing buffer (prepared as instructions on the official website of Smart-Lifesciences). The pull-down proteins were eluted with 2× SDS loading buffer and immediately boiled for 15 min. The input and eluted proteins were separated on 4 to 20% Precast PAGE gels (ACE Biotechnology) and then immunoblotted with appropriate antibodies (*42*).

Co-IP assays

For in vivo co-IP assays, proteins were extracted from the epidermal cells of *N. benthamiana* through transient co-transformation of constructs (*41*). Following experimental procedures previously described in (*42*), for in vivo co-IP assays, proteins were extracted from *Arabidopsis* inflorescence apices containing two constructs with different fluorescent labels. The plant material was grounded into powder in liquid nitrogen, and 50 μl of anti-GFP magnetic microbeads (Smart Lifesciences) were added to 1 ml of co-IP binding buffer [50 mM tris HCl (pH 8.0), 1 mM $MgCl_2$, 10 mM EDTA, 5 mM DTT, 500 mM sucrose, and 100× protease cocktail inhibitor]. After incubating at 4°C for 3 hours, samples were washed four times with the washing buffer [50 mM tris-HCl (pH 8.0), 1 mM $MgCl_2$, 10 mM EDTA, 5 mM DTT, 500 mM sucrose, and 100× protease cocktail inhibitors]. Proteins were eluted with 2× SDS loading buffer and immediately boiled for 15 min. The input and eluted proteins were separated by 4 to 20% Precast PAGE gels (ACE Biotechnology) and then immunoblotted with appropriate antibodies (*42*).

BiFC assays

Following procedures previously described in (*42*), we transformed the constructs into *A. tumefaciens* (strain GV3101) and cultured them overnight in the LB medium containing specific antibiotics. Then, we resuspended them in an infection solution [10 mM MES, 10 mM $MgCl_2$, and 200 μM acetosyringone (pH 5.8)] with an OD_{600} of 1.0. *A. tumefaciens* carrying nYFP and cYFP constructs were mixed in equal proportions and were infiltrated into the leaves of *N. benthamiana* after 3 hours in the dark. After growing in the dark for 36 hours, leaves with YFP signal were detected using confocal microscopy (*42*).

RNA-seq and data analysis

The samples for RNA-seq were collected from wild-type *Arabidopsis* under different treatment conditions (including $MgCl_2$ control, PXO99A, and PXO99A ΔTleA&B) and PUB14-related mutants (including wild-type control, *PUB14 CRISPR*, and UBQ10:PUB14-mCherry). Total RNAs were isolated from fresh inflorescence apices. More than 100 mg of inflorescence apices were collected with three biological replicates. The remaining RNA-seq procedures were carried out as previously described (*42*). Raw data have been uploaded in the Supplementary Materials and DRYAD database (https://doi.org/10.5061/dryad.jwstqjqkp).

Molecular modeling

The structures of *Arabidopsis* (wild-type PUB14-TleB, PUB14-BZR1, TleB-BZR1, and PUB14-TleB-BZR1) and PUB14-TleB-BZR1 complexes in multispecies were predicted using an AlphaFold server on the basis of AlphaFold 2.3.1 and prediction model, multimer (*27*). The generated protein data bank (PDB) files were processed using PyMOL2.1. Raw data have been uploaded in DRYAD database (https://doi.org/10.5061/dryad.jwstqjqkp).

Accession numbers

BZR1 (AT1G75080), PUB14 (AT3G54850), PUB40 (AT5G40140), BES1 (AT1G19350), ACTIN2 (AT3G18780), BAK1 (AT4G33430), BKK1 (AT2G13790), TleA (WP_240321041), TleB (WP_048488806).

Quantification and statistical analysis

Following procedures previously described in (*42*), for all experiments, statistical analyses were carried out using Microsoft Office Excel software (Microsoft Corporation, USA) and GraphPad Prism 8 (www.graphpad.com/features). Two-tailed Student's *t* tests were used to compare between two samples. For comparisons among more than two groups, Duncan's test of one-way analysis of variance (ANOVA) was used ($P < 0.05$). Data were represented as the means ± SEM from at least three independent experiments, and "*n*" represents the number of biological replicates. For quantification, the phenotypes were measured using ImageJ software (*42*). The original data have been uploaded in the Supplementary Materials.

Supplementary Materials

This PDF file includes:

Figs. S1 to S14
Table S1
Legend for data S1

Other Supplementary Material for this manuscript includes the following:

Data S1

REFERENCES AND NOTES

1. J. D. Jones, J. L. Dangl, The plant immune system. *Nature* **444**, 323–329 (2006).
2. M. Senthil-Kumar, K. S. Mysore, Nonhost resistance against bacterial pnaturathogens: Retrospectives and prospects. *Annu. Rev. Phytopathol.* **51**, 407–427 (2013).
3. Y. T. Wang, H. W. Chen, M. S. Shao, T. Zhu, S. S. Li, P. A. Olsson, E. C. Hammer, Arbuscular mycorrhizal fungi trigger danger-associated peptide signaling and inhibit carbon-phosphorus exchange with nonhost plants. *Plant Cell Environ.* **46**, 2206–2221 (2023).
4. Z. He, S. Webster, S. Y. He, Growth-defense trade-offs in plants. *Curr. Biol.* **32**, R634–R639 (2022).
5. T. L. Karasov, E. Chae, J. J. Herman, J. Bergelson, Mechanisms to mitigate the trade-off between growth and defense. *Plant Cell* **29**, 666–680 (2017).
6. S. L. Cappelli, N. A. Pichon, A. Kempel, E. Allan, Sick plants in grassland communities: A growth-defense trade-off is the main driver of fungal pathogen abundance. *Ecol. Lett.* **23**, 1349–1359 (2020).

7. T. Züst, A. A. Agrawal, Trade-offs between plant growth and defense against insect herbivory: An emerging mechanistic synthesis. *Annu. Rev. Plant Biol.* **68**, 513–534 (2017).
8. M. Gao, Y. He, X. Yin, X. Zhong, B. Yan, Y. Wu, J. Chen, X. Li, K. Zhai, Y. Huang, X. Gong, H. Chang, S. Xie, J. Liu, J. Yue, J. Xu, G. Zhang, Y. Deng, E. Wang, D. Tharreau, Z. He, Ca^{2+}sensor-mediated ROS scavenging suppresses rice immunity and is exploited by a fungal effector. *Cell* **184**, 5391–5404.e17 (2021).
9. S.-X. Yu, L.-W. Zhou, L.-Q. Hu, Y.-T. Jiang, Y.-J. Zhang, S.-L. Feng, Y. Jiao, L. Xu, W.-H. Lin, Asynchrony of ovule primordia initiation in *Arabidopsis*. *Development* **147**, dev196618 (2020).
10. L. Q. Hu, J. H. Chang, S. X. Yu, Y. T. Jiang, R. H. Li, J. X. Zheng, Y. J. Zhang, H. W. Xue, W. H. Lin, *PIN3* positively regulates the late initiation of ovule primordia in *Arabidopsis thaliana*. *PLOS Genet.* **18**, e1010077 (2022).
11. H. Y. Huang, W. B. Jiang, Y. W. Hu, P. Wu, J. Y. Zhu, W. Q. Liang, Z. Y. Wang, W. H. Lin, BR signal influences *Arabidopsis* ovule and seed number through regulating related genes expression by BZR1. *Mol. Plant* **6**, 456–469 (2013).
12. I. Bartrina, E. Otto, M. Strnad, T. Werner, T. Schmülling, Cytokinin regulates the activity of reproductive meristems, flower organ size, ovule formation, and thus seed yield in *Arabidopsis thaliana*. *Plant Cell* **23**, 69–80 (2011).
13. M. Cucinotta, L. Colombo, I. Roig-Villanova, Ovule development, a new model for lateral organ formation. *Front. Plant Sci.* **5**, 117 (2014).
14. S. H. Zu, Y. T. Jiang, J. H. Chang, Y. J. Zhang, H. W. Xue, W. H. Lin, Interaction of brassinosteroid and cytokinin promotes ovule initiation and increases seed number per silique in *Arabidopsis*. *J. Integr. Plant Biol.* **64**, 702–716 (2022).
15. M. Cucinotta, M. D. Marzo, A. Guazzotti, S. D. Folter, M. M. Kater, L. Colombo, Gynoecium size and ovule number are interconnected traits that impact seed yield. *J. Exp. Bot.* **71**, 2479–2489 (2020).
16. B. F. Li, S. X. Yu, L. Q. Hu, Y. J. Zhang, N. Zhai, L. Xu, W. H. Lin, Simple culture methods and treatment to study hormonal regulation of ovule development. *Front. Plant Sci.* **9**, 784 (2018).
17. H. Lin, M. Wang, Y. Chen, K. Nomura, S. Hui, J. Gui, X. Zhang, Y. Wu, J. Liu, Q. Li, Y. Deng, L. Li, M. Yuan, S. Wang, S. Y. He, Z. He, An MKP-MAPK protein phosphorylation cascade controls vascular immunity in plants. *Sci. Adv.* **8**, eabg8723 (2022).
18. B. D. Ondov, N. H. Bergman, A. M. Phillippy, Interactive metagenomic visualization in a Web browser. *BMC. Bioinformatics.* **12**, 385 (2011).
19. B. T. Ho, T. G. Dong, J. J. Mekalanos, A view to a kill: The bacterial type VI secretion system. *Cell Host Microbe* **15**, 9–21 (2014).
20. A. P. Macho, C. Zipfel, Targeting of plant pattern recognition receptor-triggered immunity by bacterial type-III secretion system effectors. *Curr. Opin. Microbiol.* **23**, 14–22 (2015).
21. X. Zhao, L. Gao, Q. Ali, C. Yu, B. Yuan, H. Huang, J. Long, Q. Gu, H. Wu, X. Gao, A type VI secretion system effector TseG of *Pantoea ananatis* is involved in virulence and antibacterial activity. *Mol. Plant Pathol.* **25**, e13442 (2024).
22. N. Kim, J. J. Kim, I. Kim, M. Mannaa, J. Park, J. Kim, H.-H. Lee, S.-B. Lee, D.-S. Park, W.-J. Sul, Y.-S. Se, Type VI secretion systems of plant-pathogenic *Burkholderia glumae* BGR1 play a functionally distinct role in interspecies interactions and virulence. *Mol. Plant Pathol.* **21**, 1055–1069 (2020).
23. H. Hu, H. Zhang, Z. Gao, D. Wang, G. Liu, J. Xu, K. Lan, Y. Dong, Structure of the type VI secretion phospholipase effector Tle1 provides insight into its hydrolysis and membrane targeting. *Acta Crystallogr. D Biol. Crystallogr.* **70**, 2175–2185 (2014).
24. X. Ma, L. A. N. Claus, M. E. Leslie, K. Tao, Z. Wu, J. Liu, X. Yu, B. Li, J. Zhou, D. V. Savatin, J. Peng, B. M. Tyler, A. Heese, E. Russinova, P. He, L. B. Shan, Ligand-induced monoubiquitination of BIK1 regulates plant immunity. *Nature* **581**, 199–203 (2020).
25. J. Jumper, R. Evans, A. Pritzel, T. Green, M. Figurnov, O. Ronneberger, K. Tunyasuvunakool, R. Bates, A. Žídek, A. Potapenko, A. Bridgland, C. Meyer, S. A. A. Kohl, A. J. Ballard, A. Cowie, B. Romera-Paredes, S. Nikolov, R. Jain, J. Adler, T. Back, S. Petersen, D. Reiman, E. Clancy, M. Zielinski, M. Steinegger, M. Pacholska, T. Berghammer, S. Bodenstein, D. Silver, O. Vinyals, A. W. Senior, K. Kavukcuoglu, P. Kohli, D. Hassabis, Highly accurate protein structure prediction with AlphaFold. *Nature* **596**, 583–589 (2021).
26. L. L. Presti, D. Lanver, G. Schweizer, S. Tanaka, L. Liang, M. Tollot, A. Zuccaro, S. Reissmann, R. Kahmann, Fungal effectors and plant susceptibility. *Annu. Rev. Plant Biol.* **66**, 513–545 (2015).
27. J. Fan, X. Y. Guo, L. Li, F. Huang, W. X. Sun, Y. Li, Y. Y. Huang, Y. J. Xu, J. Shi, Y. Lei, A. P. Zheng, W. M. Wang, Infection of *Ustilaginoidea virens* intercepts rice seed formation but activates grain-filling-related genes. *J. Integr. Plant Biol.* **57**, 577–590 (2015).
28. G.-B. Li, J.-X. He, J.-L. Wu, H. Wang, X. Zhang, J. Liu, X.-H. Hu, Y. Zhu, S. Shen, Y.-F. Bai, Z.-L. Yao, X.-X. Liu, J.-H. Zhao, D.-Q. Li, Y. Li, F. Huang, Y.-Y. Huang, Z.-X. Zhao, J.-W. Zhang, S.-X. Zhou, Y.-P. Ji, M. Pu, P. Qin, S.-G. Li, X.-W. Chen, J. Wang, M. He, W. Li, X.-J. Wu, Z.-J. Xu, W.-M. Wang, J. Fan, Overproduction of OsRACK1A, an effector- targeted scaffold protein promoting OsRBOHB-mediated ROS production, confers rice floral resistance to false smut disease without yield penalty. *Mol. Plant* **15**, 1790–1806 (2022).
29. J. H. Chang, D. Desveaux, A. L. Creason, The ABCs and 123s of bacterial secretion systems in plant pathogenesis. *Annu. Rev. Phytopathol.* **52**, 317–345 (2014).
30. R. E. Hernandez, R. Gallegos-Monterrosa, S. J. Coulthurst, Type VI secretion system effector proteins: Effective weapons for bacterial competitiveness. *Cell. Microbiol.* **22**, e13241 (2020).
31. F. Jiang, N. R. Waterfield, J. Yang, G. Yang, Q. Jin, A *Pseudomonas aeruginosa* type VI secretion phospholipase D effector targets both prokaryotic and eukaryotic cells. *Cell Host Microbe* **15**, 600–610 (2014).
32. E.-J. Kim, S.-H. Lee, C.-H. Park, S.-H. Kim, C.-C. Hsu, S. Xu, Z.-Y. Wang, S.-K. Kim, T.-W. Kim, Plant u-box40 mediates degradation of the brassinosteroid-responsive transcription factor BZR1 in *Arabidopsis* roots. *Plant Cell* **31**, 791–808 (2019).
33. L. B. Kumagai, P. W. Woods, R. Walcott, X. Moua, First report of bacterial fruit blotch on Melon caused by *Acidovorax citrulli* in California. *Plant. Dis.* **98**, 1423–1423 (2014).
34. W. Yang, Y. H. Ju, L. Zuo, L. Shang, X. Li, X. Li, S. Feng, X. Ding, Z. Chu, OsHsfB4d binds the promoter and regulates the expression of *OsHsp18.0-CI* to resistant against *Xanthomonas oryzae*. *Rice.* **13**, 28 (2020).
35. W. Huang, A. M. MacLean, A. Sugio, A. Maqbool, M. Busscher, S.-T. Cho, S. Kamoun, C.-H. Kuo, R. G. H. Immink, S. A. Hogenhout, Parasitic modulation of host development by ubiquitin-independent protein degradation. *Cell* **184**, 5201–5214.e12 (2021).
36. P. Bernal, L. P. Allsopp, A. Filloux, M. A. Llamas, The *Pseudomonas putida* T6SS is a plant warden against phytopathogens. *ISME J.* **11**, 972–987 (2017).
37. L. S. Ma, A. Hachani, J. S. Lin, A. Filloux, E. M. Lai, *Agrobacterium tumefaciens* deploys a superfamily of type VI secretion DNase effectors as weapons for interbacterial competition in planta. *Cell Host Microbe* **16**, 94–104 (2014).
38. F. R. Cianfanelli, L. Monlezun, S. J. Coulthurst, Aim, load, fire: The type VI secretion system, a bacterial nanoweapon. *Trends Microbiol.* **24**, 51–62 (2016).
39. G. Wang, X. Chen, C. Yu, X. Shi, W. Lan, C. Gao, J. Yang, H. Dai, X. Zhang, H. Zhang, B. Zhao, Q. Xie, N. Yu, Z. He, Y. Zhang, E. Wang, Release of a ubiquitin brake activates OsCERK1-triggered immunity in rice. *Nature* **629**, 1158–1164 (2024).
40. M. Gao, Z. Hao, Y. Ning, Z. He, Revisiting growth-defence trade-offs and breeding strategies in crops. *Plant Biotechnol. J.* **22**, 1198–1205 (2024).
41. R. Wang, R. Wang, M. Liu, W. Yuan, Z. Zhao, X. Liu, Y. Peng, X. Yang, Y. Sun, W. Tang, Nucleocytoplasmic trafficking and turnover mechanisms of BRASSINAZOLE RESISTANT1 in *Arabidopsis thaliana*. *Proc. Natl. Acad. Sci. U.S.A.* **118**, e2101838118 (2021).
42. Y. T. Jiang, L. H. Yang, J. X. Zheng, X. C. Geng, Y. X. Bai, Y. C. Wang, H. W. Xue, W. H. Lin, Vacuolar H^+-ATPase and BZR1 form a feedback loop to regulate the homeostasis of BR signaling in *Arabidopsis*. *Mol. Plant* **16**, 1976–1989 (2023).
43. S. J. Clough, A. F. Bent, Floral dip: A simplified method for *Agrobacterium*-mediated transformation of *Arabidopsis thaliana*. *Plant J.* **16**, 735–743 (1998).
44. T. Murashige, F. Skoog, A Revised Medium for Rapid Growth and Bio Assays with Tobacco Tissue Cultures. *Physiol. Plant.* **15**, 473–497 (1962).
45. D. H. Zheng, X. Y. Yao, M. Duan, Y. F. Luo, B. Liu, P. Y. Qi, M. Sun, L. F. Ruan, Two overlapping two-component systems in *Xanthomonas oryzae* pv. *oryzae* contribute to full fitness in rice by regulating virulence factors expression. *Sci. Rep.* **6**, 22768 (2016).
46. H. L. Xing, L. Dong, Z. P. Wang, H. Y. Zhang, C. Y. Han, B. Liu, X. C. Wang, Q. J. Chen, A CRISPR/Cas9 toolkit for multiplex genome editing in plants. *BMC Plant Biol.* **14**, 327 (2014).
47. N. M. Springer, Isolation of plant DNA for PCR and genotyping using organic extraction and CTAB. *Cold Spring Harb. Protoc.* **2010**, pdb.prot5515 (2010).
48. S. Chen, Y. Zhou, Y. Chen, J. Gu, fastp: An ultra-fast all-in-one FASTQ preprocessor. *Bioinformatics* **34**, i884–i890 (2018).
49. B. Langmead, S. L. Salzberg, Fast gapped-read alignment with Bowtie 2. *Nat. Methods* **9**, 357–359 (2012).
50. W. Li, A. Godzik, Cd-hit: A fast program for clustering and comparing large sets of protein or nucleotide sequences. *Bioinformatics* **22**, 1658–1659 (2006).
51. W. Zhu, A. Lomsadze, M. Borodovsky, Ab initio gene identification in metagenomic sequences. *Nucleic Acids Res.* **38**, e132 (2010).
52. D. Kurihara, Y. Mizuta, Y. Sato, T. Higashiyama, ClearSee: A rapid optical clearing reagent for whole-plant fluorescence imaging. *Development* **142**, 4168–4179 (2015).
53. Y. J. M. Liew, Y. K. Lee, N. Khalid, N. A. Rahman, B. C. Tan, Cell-free expression of a plant membrane protein BrPT2 from *Boesenbergia Rotunda*. *Mol. Biotechnol.* **63**, 316–326 (2021).
54. L. Zhang, X. Xia, M. Zhang, Y. Wang, G. Xing, X. Yin, L. Song, F. He, L. Zhang, Integrated analysis of genomics and proteomics reveals that CKIP-1 is a novel macrophage migration regulator. *Biochem. Biophys. Res. Commun.* **436**, 382–387 (2013).
55. Y. Zhang, Y. J. Zhang, B. J. Yang, X. X. Yu, D. Wang, S. H. Zu, H. W. Xue, W. H. Lin, Functional characterization of *GmBZL2* (*AtBZR1* like gene) reveals the conserved BR signaling regulation in *Glycine max*. *Sci. Rep.* **6**, 31134 (2016).

Acknowledgments: We thank W.-Q. Tang from Hebei Normal University for constructive discussion and providing vectors pBZR1:BZR1-YFP and J.-B. Fan, G.-Z. Wu, W.-Q. Liang, Y. Bao, G. Yu, Y.-N. Hou, G.-Y. Chen, Y.-S. Lin, G.-Q. Chen, J. Pan, and L.-F. Zou from Shanghai Jiao Tong University for providing plant and bacterial materials. The computations here were run on the Siyuan-1 cluster supported by the Center for High-Performance Computing at Shanghai Jiao

Tong University. **Funding:** This research was supported by funding from the National Natural Science Foundation of China (32270339 and 92354301), the Scientific and Technological Innovation Action Program of Shanghai (23JC1402800), and the Agri-X Interdisciplinary Fund of Shanghai Jiao Tong University (Agri-X20200204). **Author contributions:** Writing—original draft: W.-H.L., T.D., T.-D.X., J.-T.Y., Z.-M.T., Y.-T.J., and Y.-X.B. Writing—review and editing: W.-H.L., T.-D.X., J.-T.Y., Z.-M.T., and Y.-T.J. Conceptualization: W.-H.L., T.D., T.-D.X., H.-W.X., J.-T.Y., and Y.-T.J. Investigation: W.-H.L., T.D., J.-T.Y., Z.M.T., Y.-T.J., Y.-X.B., and Y.-J.Z. Visualization: W.-H.L., J.-T.Y., Y.-T.J., and Y.-X.B. Methodology: W.-H.L., T.D., J.-T.Y., and Y.-X.B. Resources: W.-H.L., T.D., J.-T.Y., Z.-M.T., Y.-T.J., and Y.-X.B. Validation: W.-H.L., J.-T.Y., Z.-M.T., Y.-T.J., and Y.-J.Z. Supervision: W.-H.L., T.D., and J.-T.Y. Formal analysis: W.-H.L., J.-T.Y., Z.-M.T., Y.-X.B., and Y.-J.Z. Project administration: W.-H.L., T.D., J.-T.Y., and Z.-M.T. Funding acquisition: W.-H.L., T.D., and J.-T.Y. Data curation: W.-H.L., T.D., and J.-T.Y. Software: J.-T.Y., and Y.-X.B. **Competing interests:** The authors declare that they have no competing interests. **Data and materials availability:** All data needed to evaluate the conclusions in the paper are present in the paper, the Supplementary Materials, and DRYAD database (https://doi.org/10.5061/dryad.jwstqjqkp).

Submitted 27 August 2024
Accepted 4 December 2024
Published 8 January 2025
10.1126/sciadv.ads7738